Programmable Living Units for Emulating Pancreatic Tumor-Stroma Interplay

Maria V. Monteiro, Marta Rocha, Vítor M. Gaspar*, João F. Mano*

M. V. Monteiro, M. Rocha, V.M. Gaspar, J.F. Mano
Department of Chemistry, CICECO – Aveiro Institute of Materials, University of Aveiro
Campus Universitário de Santiago, 3810-193, Aveiro, Portugal
*Corresponding authors:
E-mail: vm.gaspar@ua.pt, jmano@ua.pt

Keywords: superhydrophobic surfaces, 3D *in vitro* tumor models, pancreatic tumor microenvironment, preclinical drug screening

Abstract

Bioengineering close-to-native *in vitro* models that emulate tumors bioarchitecture and microenvironment is highly appreciable for improving disease modelling toolboxes. Herein, pancreatic cancer living units – so termed cancer-on-a-bead models - were generated. Such user-programmable *in vitro* platforms exhibit biomimetic multi-compartmentalization and tunable integration of cancer associated stromal elements. These stratified units can be rapidly assembled in-air, exhibit reproducible morphological features, tunable size, and recapitulate spatially resolved tumor-stroma ECM niches. Compartmentalization of pancreatic cancer and stromal cells in well-defined ECM microenvironments stimulated the secretion of key biomolecular effectors including TGF-β and IL-1β, closely emulating the signatures of human pancreatic tumors. Cancer-on-a-bead models also display increased drug resistance to chemotherapeutics when compared to their reductionistic counterparts, reinforcing the importance to differentially model ECM components inclusion and their spatial stratification as observed *in vivo*. Beyond providing a universal technology that enables spatial modularity in tumor-stroma elements bioengineering, this study provides a scalable, in-air fabrication of ECM-tunable 3D platforms that can be leveraged for recapitulating differential matrix composition occurring in other human neoplasia's.

1. Introduction

Engineering predictive and robust *in vitro* tumor models that fully recapitulate native human tumors pathophysiological traits in a controlled *in vitro* setting is crucial to accelerate the discovery and validation of innovative therapeutics.[1,2] Up-to-date the pipeline of advanced therapeutics for human malignancies has been hindered by the lack of preclinical cancer models that recapitulate key tumor microenvironment (TME) hallmarks and pathophysiological features, resulting in poor correlation with human clinical trials.[3,4]

Recent endeavors have actively sought to better recapitulate human tumors via bioengineering of evermore advanced 3D *in vitro* models, including: (i) 3D spheroids, (ii) organoids, (iii) ECM-mimetic hydrogel-based platforms, (iv) porous based scaffolds or (v) microfluidic chip systems, which better emulate key hallmarks of human cancers.[5–13] Such platforms have undoubtedly opened a wide range of opportunities for recapitulating tumor biomolecular signatures, unravel intricate cell-cell interplays and modulate different TME components (i.e., cell populations and the supportive tumor extracellular matrix (ECM)). Despite their major contribution for improving preclinical drug screening, current 3D models ability for seamlessly mimicking human tumor specific bioarchitecture, the differential cells and ECM spatial organization is still limited and underexplored.

Clinical evidences indicate that various neoplasia's (e.g., breast, lung, brain, or pancreas) naturally display spatially resolved cellular distributions during their progression and maturation. Among these, pancreatic ductal adenocarcinoma (PDAC) is one of the most deadly and challenging to emulate owing to its dense and desmoplastic stroma generally distributed in a juxtatumoral position, ultimately enveloping tumor cells.[14–20] Natively, PDAC stroma is populated by various stromal cells (e.g., cancer-associated fibroblasts (CAFs), tumor-associated macrophages, etc.), which display key roles in tumor progression and resistance. PDAC is also characterized by abundant *de novo* secretion of ECM components (e.g., collagen, hyaluronic acid, fibronectin, etc.) a major hallmark of this malignancy and that is mainly attributed to highly active myofibroblast CAFs present in its microenvironment.[21–23]

Considering the importance of such unique tumor-stroma niche in the resistance to therapeutics, evermore evolved 3D *in vitro* models are currently under development for recapitulating PDAC unique bioarchitecture and active stroma in an attempt to bioengineer more physiomimetic models.[24] Recently, we generated heterotypic 3D PDAC stratified microenvironment spheroid models – so termed STAMS – comprising pancreatic cancer cells and CAFs organized in a stratified mode aiming to reproduce PDAC niche key signatures.[5] These platforms were highly robust in mirroring the desmoplastic reaction, stratified

architecture and drug resistance in a controlled laboratory setting.[5] Yet, the development of living pancreatic cancer models comprising pre-existing ECM components, namely tumor-specific and stroma-specific ECM in a relevant stratified spatial organization remains to be addressed.

Considering ECM's role in tumor progression and drug resistance, herein, we leveraged on superhydrophobic surfaces to generate compartmentalized pancreatic tumor-stroma living units that enable user-programmable PDAC TME elements incorporation by simple selection of the cell types/density and biomaterials to include in superhydrophobic platforms for generating the compartmentalized 3D tumor models. Such cancer-on-a-bead platforms present a core-shell architecture with: (i) a tumor-ECM core (i.e., cancer cells laden in a methacrylated gelatin (GelMA) hydrogel matrix) and (ii) a juxtatumoral stromal-ECM compartment (i.e., cancer-associated fibroblasts laden in GelMA and methacrylated hyaluronan (HA-MA) highly rich hydrogel matrix).

Such in-air assembled living unit beads enabled a tunable distribution of ECM mimetic components and the modulation of fibrotic elements density, unlocking a wide range of possible 3D tumor-stroma combinations that capture different desmoplastic states of pancreatic cancer opening new avenues to study stroma-related events. The significance and biomimicry potential of such 3D models was corroborated by their ability for resembling human tumor cells-ECM spatial organization, biomolecular signatures, and drug resistance. Overall, the developed cancer-on-a-bead platforms were highly reproducible and amenable for high-throughput/high-content imaging. Alongside, their inherent user-programmable features support their potential to be harnessed for modelling other human neoplasia's that may also exhibit such stratified tumor microenvironment bioarchitectures.

2. Results and discussion

The tunable fabrication of 3D *in vitro* tumor models that resemble key tumor ECM components and cellular signatures remain in high demand to overcome the widely used, and yet, overly simplistic 2D preclinical platforms. Exploring ECM-mimetic matrices and fast hydrogel processing technologies that provide design freedom for bioengineering physiomimetic tumor-stroma models can contribute for expanding the toolbox of current preclinical screening platforms. PDAC is generally characterized by a unique spatial cell distribution in which ductal cancer cells are enveloped by a dense and fibrotic stroma comprising stromal cells, mainly CAFs, and abundant ECM (**Scheme 1**).[17,25] Adding to this, recent evidences obtained from high-throughput proteomics analysis further indicate a

differential distribution of ECM components between cancer cells niche (i.e., mainly rich in collagen) and their juxtatumoral stroma compartment (i.e., mostly rich in collagen and hyaluronan).[26]

To mimic this intricate microenvironment and bioarchitecture, we leveraged on superhydrophobic platforms for rapidly fabricating fully user-programable pancreatic tumor-stroma core-shell 3D hydrogel units that recapitulate native spatial and matrix stratification. In fact, to date a number of approaches have been followed to fabricate compartmentalized hydrogel beads including, double-emulsion strategies, electrospray and superhydrophobic surfaces.[27–33] The later comprises the deposition of a polymeric solution on the superhydrophobic surface forming a spherically shaped droplet while avoiding the use of solvents. Besides being an organic solvent free strategy, superhydrophobic surfaces are cost-effective, easily handleable and enable to produce polymeric beads of different sizes and with spherical-like morphologies, dependent on the droplet volume and polymer concentration.[34] To rationally select the biomaterials to include we followed a top-down deconstructive approach that considers the main cellular and ECM elements of this tumor.

Particularly, Collagen and hyaluronan (HA) have been reported to be overexpressed in human PDAC.[35] Increasing evidences have suggested that HA, a negatively charged non-sulfated glycosaminoglycan (GAG), is abundantly accumulated in tumor surrounding stroma, contributing to an extensive desmoplastic reaction.[36,37] Although the process by which HA accumulated in PDAC stroma is still under investigation, recent proteomic and genomic-based evidences have demonstrated that while both cancer cells and CAFs produce increasing levels of collagens, it was verified that HA is mostly overexpressed by CAFs and it is highly concentrated in the stromal region.[26,36,38] Interestingly, owing to HA role in fibrotic stroma establishment and hampering anti-cancer drugs delivery, efforts are being made focus on targeting this stroma component by administration of HA-targeting enzymatic agent.[39] Consequently, as HA-rich stroma has been highly correlated with tumor progression, invasion, resistance and poor patients outcome, cancer-on-a-bead was designed to resemble such ECM and cellular stratification, being a promising platform to study tumor-stroma cooperative relationship and anti-cancer therapies targeting the unique and pro-tumoral PDAC stroma. On the other hand, Collagen I (Col I) is the most abundant ECM protein found in native PDAC and its stroma, being abundantly secreted by tumor-associated cells and actively participates in cell proliferation, invasion and metastasis, contributing to the ineffectiveness of tumor-targeting therapies.[40] Herein, collagen matrix was emulated by using gelatin-based hydrogels. Gelatin-based platforms, derived from collagen hydrolysis, have been widely used to establish 3D

disease models.[1,41–44] Despite gelatin lacks the ability to form fibrillar structures achieved with collagen, this protein-based biomaterial exhibits collagen-like properties such as biocompatibility and biodegradation with the advantage of its lower cost and easy chemical modification. Particularly, gelatin has been widely modified with methacrylated groups to produce photocrosslinked biomaterials.[7,13,44–46] The mechanical properties of the obtained hydrogels can also be easily tailored by varying the degree of modification, polymer concentration, gelation time or photocrosslinking agent concentration. Owing to its valuable properties, gelatin-based hydrogels including methacrylated gelatin (GelMA) have been widely applied to study angiogenesis, tumor growth and drug resistance in a preclinical setting. Additionally, GelMA can be combined with other (bio)polymers to produce complex ECM-mimetic matrices that more closely emulate the native TME.

For emulating PDAC hallmarks, herein we engineered: (i) the tumor core comprising malignant pancreatic cancer cells and its most abundant ECM element, (ii) the cellular spatial organization in which CAFs are localized in a juxta-tumoral position, encasing cancer cells and its specific ECM, and (iii) the stratified bioarchitecture of this tumor by generating core-shell living units (Scheme 1). The 3D tumor core was thus comprised by cancer cells laden in GelMA, representing the abundant collagen content found in PDAC malignant niche, while the stroma compartment encompasses CAFs laden in GelMA/HAMA hydrogels, aiming to reproduce the characteristic fibrotic stroma niche.

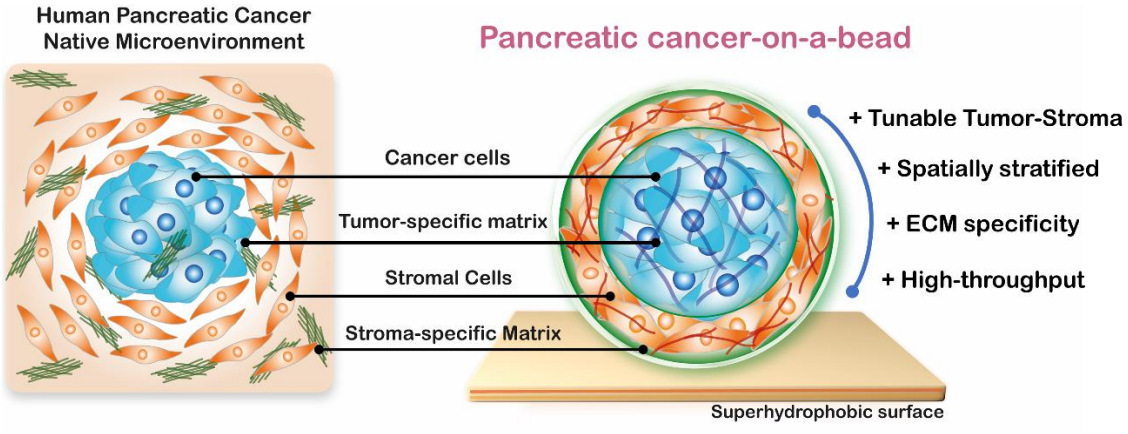

Scheme 1. Infographic of pancreatic cancer-on-a-bead technology that operates as a physiomimetic *in vitro* model to recapitulate major pancreatic cancer tumor microenvironment hallmarks. These features open new opportunities to target different disease promoting biological pathways and barriers that are unique to this neoplasia. Herein we propose the use of superhydrophobic surfaces to rapidly fabricate stratified living hydrogels comprising pancreatic

ductal adenocarcinoma cellular elements (i.e., cancer and stromal cells), its compartment specific ECMs and their differential spatially stratification as observed *in vivo,* enabling an unprecedented level of tunability of the fibrotic elements and biomimicry to the *in vivo* setting. This reproducible and totally organic-solvent free approach renders cancer-on-a-bead living models highly amenable for large scale fabrication in-air and their translation to different screening procedures that benefit from high-throughput/high-content imaging analysis.

2.1. Bioengineered living unit tumor-stroma models

Initially, we aimed to evaluate the potential of superhydrophobic surfaces to fabricate tunable 3D core-shell pancreatic cancer-on-a-bead models in-air and in a totally organic/oil solvent-free approach that are generally required in other assembly strategies (i.e., emulsion, microfluidic platforms). For this, core and shell compartments volumes were tuned to investigate the effect of digitally dispensed volume on hydrogel beads size (**Figure 1A-E**).

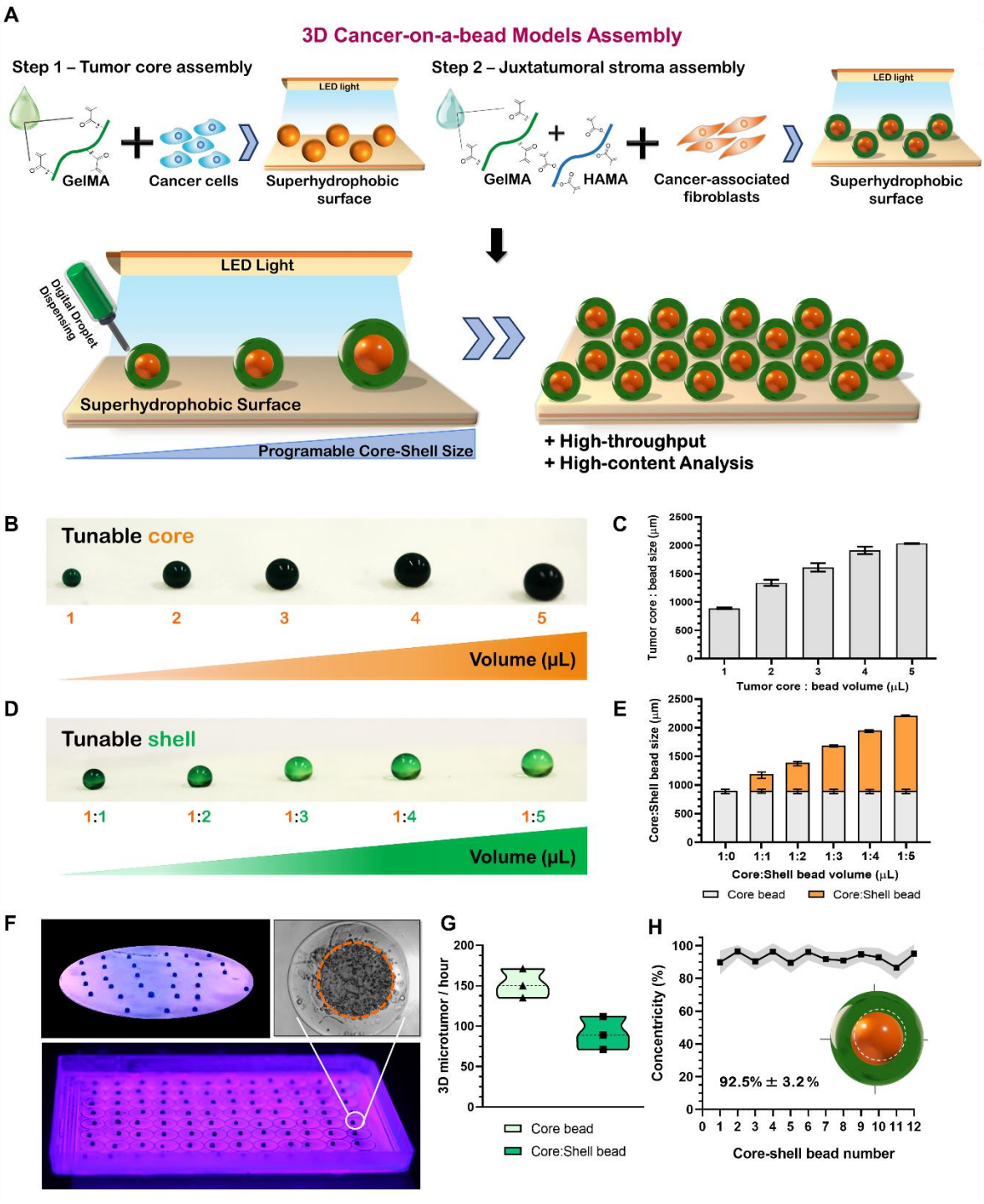

Figure 1. Characterization of tunable core-shell ECM-mimetic unit models. (A) Schematics of biomimetic hydrogel models generation with programable core-shell size. Modulation of (B,C) core and (D,E) shell unit compartments via increasing GelMA and GelMA-HAMA hydrogel volumes through controlled digital dispensing. (C,E) Both tumor and core-shell hydrogel beads size increases with the deposited volume, while the produced units maintain their quasi-spherical morphology highlighting the potential of this platform to generate tumor-stroma cancer-on-a-bead models with tunable ECM compartments. Data is presented as mean ± s.d., *n*= 3. (F) Digital photographs demonstrating in-air generation of core-shell beads, either in indentation-free superhydrophobic disc platforms and in a 96-spot array plate. (G) Core-shell hydrogel units production rate considering hydrogel loading-dispensing-photocrosslinking-

manipulation cycle times. (H) concentricity analysis of core-shell tumor-stroma ECM-mimetic units. Data is presented as mean ± s.d.

To establish the tumor compartment, (GelMA) core beads with different volumes (1-5 µL) were generated and photocrosslinked with visible light (λ= 406 nm) (**Figure 1B**). The results demonstrated that core units size increases with the deposited volume, enabling a precise tunning of the core compartment size and the cell density to be included (**Figure 1C**). Compartmentalized core-shell beads with different GelMA:HAMA shell volumes were also generated via digital droplet spotting and visible light mediated photocrosslinking (**Figure 1D and supplementary VideoS1**). The results demonstrated that core-shell units size produced in superhydrophobic surfaces also increased with the deposited shell volume (**Figure 1E**). The latter is highly relevant and may unlock the possibility to mimic different PDAC fibrotic states by simply dispensing more ECM and seeding a higher density of stromal CAFs.

Aiming to validate the ability of superhydrophobic surfaces to produce core-shell models with tunable ECM and fibrotic elements, living 3D core-shell models were then established by modulating the volume and cellular density of the stroma compartment (**Figure S1**). The results showed the ability of the developed platform to generate PDAC tumor-stroma models with tunable stroma compartments where cells attach and survive within the ECM-mimetic hydrogel independently of the shell volume or stroma cellular density. This methodology can offer an increased potential to explore numerous tumor-associated events such as the tumor-immune system interaction, as well as the intrusion of the immune cells throughout the malignant tissue, by simply manipulating the cell type to be included in each ECM.

Besides the close similarity with human tumors, preclinical tumor platforms must be amenable to high-throughput assays such as the screening and validation of therapies. To further demonstrate the compatibility of the superhydrophobic surfaces with high-throughput assays, stratified core-shell beads were generated in hydrophobized indentation-free surfaces and 96 array spot plates (**Figure 1F**). The capacity to centralize the core bead within the shell compartment as well as the producing time of both core and core-shell beads were evaluated (**Figure 1G,H**). The obtained results highlight the ability of accurately producing a significant number of PDAC models (152 core-shell beads/hour) with an average core concentricity of 92.5 % ± 3.2 %, representing a valuable technology for PDAC *in vitro* modelling.

In general, the superhydrophobic surfaces demonstrated to be suitable for producing tunable tumor-stroma models with different sizes and with spatial freedom of ECM deposition allowing an unprecedented tunning of tumor and stroma ECM properties and components. Moreover, it

allows to uncouple the tumor and stroma compartment from one another, truly representing the *in vivo* scenario and offering the possibility to tune it according to the desired applications.

2.2. Fabrication and characterization of tumor-stroma PDAC models

Aiming to validate core-shell tumor-stroma pancreatic cancer-on-a-bead units potential, three different 3D PDAC platforms were then assembled: (i) standard scaffold-free monotypic 3D PDAC spheroids established through liquid overlay technique (LOT) comprising a PANC-1 human pancreatic ductal adenocarcinoma cell line; (ii) heterotypic PDAC stratified tumor microenvironment spheroid models so termed – STAMS - in which a PANC-1 tumor mass is engulfed by CAFs cells in order to simulate the native tumor bioarchitecture and the juxta-tumoral position of CAFs, as found *in vivo, but being devoid of* any previous ECM component; and, (iii) heterotypic stratified pancreatic cancer-on-a-bead model established by using superhydrophobic surfaces, in which a PANC-1:GelMA tumor core is assembled and then surrounded by a second GelMA:HAMA shell laden with CAFs to simulate the tumor bioarchitecture and cell/ECM spatial organization.

The different 3D PDAC models were then monitored over time to evaluate 3D microtumors size and circularity. **Figure 2** demonstrates that the different 3D PDAC models maintained the stability over 14 days of culture, with the 3D stratified pancreatic cancer-on-a-bead system presenting the high circularity and maintaining microtumor size during the culture time with minimum differences between core-shell units. Such features are particularly important in drug screening assays avoiding the large variations provided by tumor spheroids in morphology and size. In addition, core-shell tumor-stroma units revealed increased robustness compared to their scaffold-free counterparts, being easily manipulated, and handled without risk of microtissue disruption, surpassing these limitations generally observed for standard tumor spheroids.

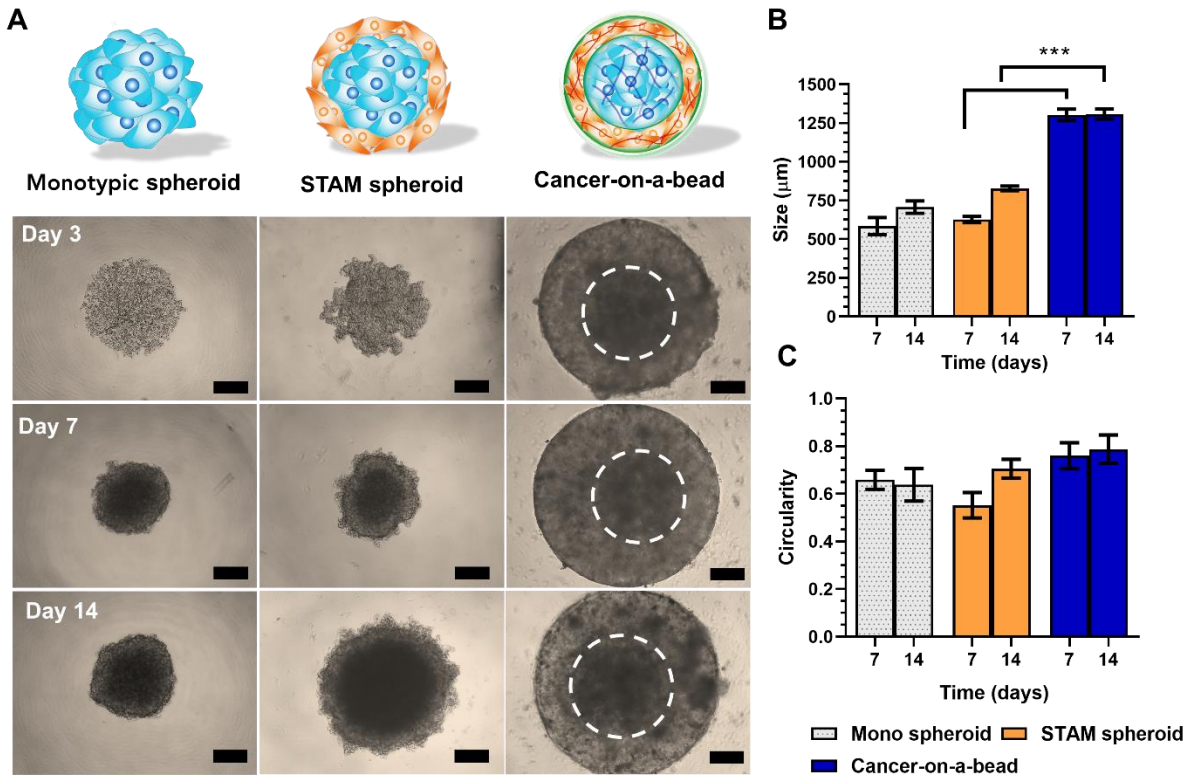

Figure 2. Characterization of 3D PDAC models. (A) Representative optical contrast micrographs of monotypic PANC-1 spheroids, STAM spheroids and stratified pancreatic cancer-on-a-bead units at days 3, 7 and 14 of culture. Scale bars = 500 µm. Evaluation of morphometric parameters: (B) size and (C) circularity of 3D tumor models over time. Data is presented as mean ± s.d., *n*=5, p***<0.001.

2.3. Cellular distribution in 3D PDAC Models

To visualize the stratified cellular organization of cancer and stromal cells in tumor-stroma 3D cancer-on-a-bead living units and verify the successful compartmentalization of PDAC stroma elements, PANC-1 and CAFs were labelled with long term cell tracking lipophilic dyes (Vybrant™ DiO and DiD, respectively). Bioimaging analysis revealed differential spatial organization of tumor and stromal compartments in the core-shell bead in which despite some cancer cells are present in shell after 14 days of culture, they are mainly localized in the core region. Otherwise, CAFs:stroma ECM are distributed and compartmentalized in the outer bead recapitulating the stroma juxtatumoral position found in native PDAC bioarchitecture (**Figure 3**). Interestingly, after 14 days of culture it is also possible visualize CAFs myofibroblast phenotype, an important aspect of PDAC stroma.

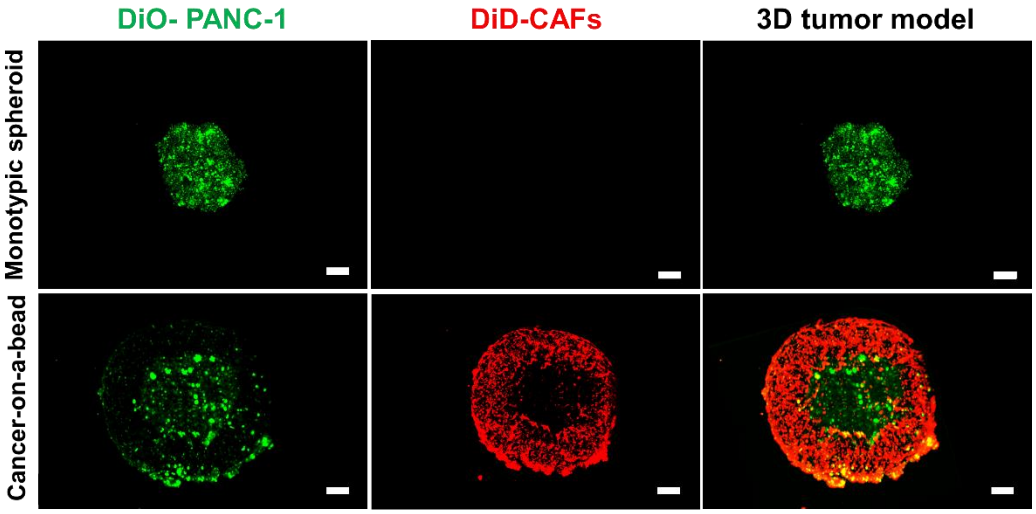

Figure 3. Widefield fluorescence micrographs of cellular spatial organization in monotypic and heterotypic microtumors, at day 14. A clear stratification and differential spatial organization is observed in cancer-on-a-bead PDAC living units with the outer stroma bead enveloping the PANC-1 tumor core bead. Such organization resembles that found in human PDAC tumors where CAFs are in direct contact with cancer cells in the periductal region.[47] DiO labelled PANC-1 cancer cells –green channel; DiD labelled CAFs-red channel. Scale bar = 300 µm.

2.4. Stratified PDAC 3D models viability

To further characterize cancer-on-a-bead living units, live/dead and metabolic activity assays were performed (**Figure 4 and S2**). Interestingly, both 3D heterotypic PDAC models showed increased viability compared to the monotypic model, highlighting CAFs role in cancer cells survival via paracrine secretion of key growth factors and cytokines. Despite STAMS model appears to present lower necrotic core than cancer-on-a-bead platforms (**Figure 4 and S2**), the later provides a more biomimetic and representative tumor model since it comprises ECM-mimetic supporting matrices. In fact, the inclusion of ECM-mimetic biomaterials in cancer-on-a-bead models provides tumor-associated cells with biochemical and biophysical cues, as demonstrated by biomolecular assays, and adds a diffusional barrier, translating into increased drug resistance. Cancer-on-a-bead models provide a unique platform to evaluate PDAC behavior, cell-stroma interactions and to screen anti-cancer or stroma therapeutics, constituting a more realistic *in vitro* model in comparison to scaffold-free 3D STAMS. Moreover, cancer-on-a-bead models are envisioned to provide the opportunity for screening other therapeutics specifically targeting tumor ECM (e.g., hyaluronidase), an approach that is being evaluated in preclinical trials and that cannot be evaluated in standard STAMS. Overall, the inclusion of stratified ECM-mimetic compartments supports the maintenance of cancer-on-a-bead platforms over 14 days and triggers the existence of necrotic spots (**Figure 4**). Necrotic regions presence is in line with the native PDAC microenvironment where generally ECM deposition by CAFs

leads to the formation of physical barriers that limit nutrients and oxygen diffusion, promoting an hypoxic TME.

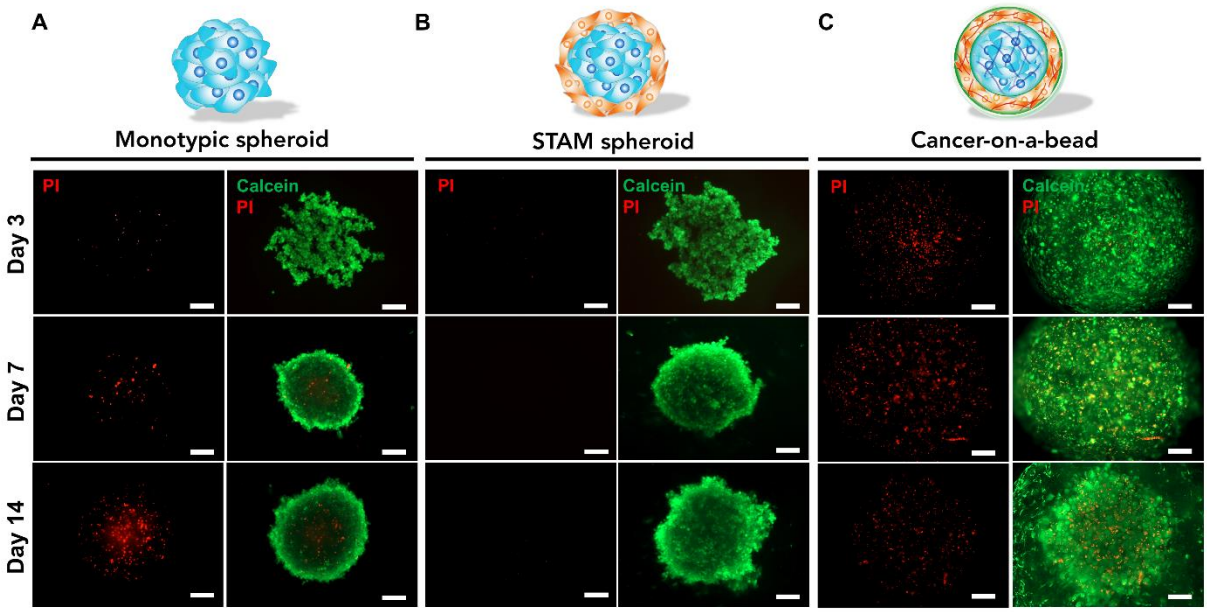

Figure 4. Widefield fluorescence micrographs of Live/Dead assays performed at 3, 7 and 14 days of culture in: (A) monotypic PANC-1 spheroids, (B) heterotypic STAMS model, and (C) heterotypic tumor-stroma 3D pancreatic cancer-on-a-bead living units. Cell viability analysis along time indicates the presence of living and necrotic elements scattered in the bead volume. Green channel: Calcein-AM, Red channel: PI. Scale bar = 250 µm.

2.5. Fibrotic stromal CAFs characterization modulation via compartmentalization

Aiming to further characterize the cellular distribution and stromal spatial arrangement in 3D pancreatic cancer-on-a-bead units, stromal CAFs morphometric features were evaluated. At early time points, CAFs laden in the hydrogel shell exhibited a rounded shape (day 1, **Figure S3)**. Whereas at 7 days of *in vitro* maturation CAFs acquired an *in vivo*-like fusiform morphology with a clear cell spreading being obtained. These findings corroborate the establishment of a suitable ECM mimetic compartment (i.e., GelMA-HAMA outer shell) for maturation of such stromal elements with CAFs cells exhibiting the characteristic myofibroblastic-like fusiform morphology with well-defined actin filaments being observed (**Figure 5 B-E)**.

Adding to this we aimed to demonstrate the versatility of cancer-on-a-bead platforms to modulate both cell density and ECM content in the stroma region. The unique user-defined programmability of the core and shell compartments in cancer-on-a-bead models enabled a straightforward fabrication of different fibrotic environments *in vitro*, as demonstrated by modelling CAFs cells density and stroma volume in the shell compartment (**Figure 5 A-G**). In fact, to date *in vitro* PDAC fibrosis tunability has been studied using 2D stacked models that

do not enable to fully recapitulate 3D tumors microenvironment.[48–50] Therefore, cancer-on-a-bead platforms revealed to be highly relevant since it opens the unique opportunity to rapidly model PDAC tumors with tunable fibrotic components, a highly sought after feature in PDAC *in vitro* models development, since this desmoplastic microenvironment is recognized to play a major role in disease progression and drug resistance. High resolution bioimaging of cancer-on-a-bead living units also shows a clear distribution of CAFs along the outer shell of these platforms. At higher CAFs densities ($1x10^5$ cells) the establishment of cellular agglomerates is clearly visible in the shell (**Figure 5 E and G**), as opposite, lower CAFs density in the outer shell originates void hydrogel sections where no cells are present (**Figure 5 B and F**). Overall, the tunability provided by cancer-on-a-bead model may offer the possibility to modulate different PDAC fibrotic states, study fibrotic stroma fibrosis-related events in future studies and administrate fibrosis inducers (e.g., TGF-β and FGF-2) or modulating matrix stiffness.[48–50]

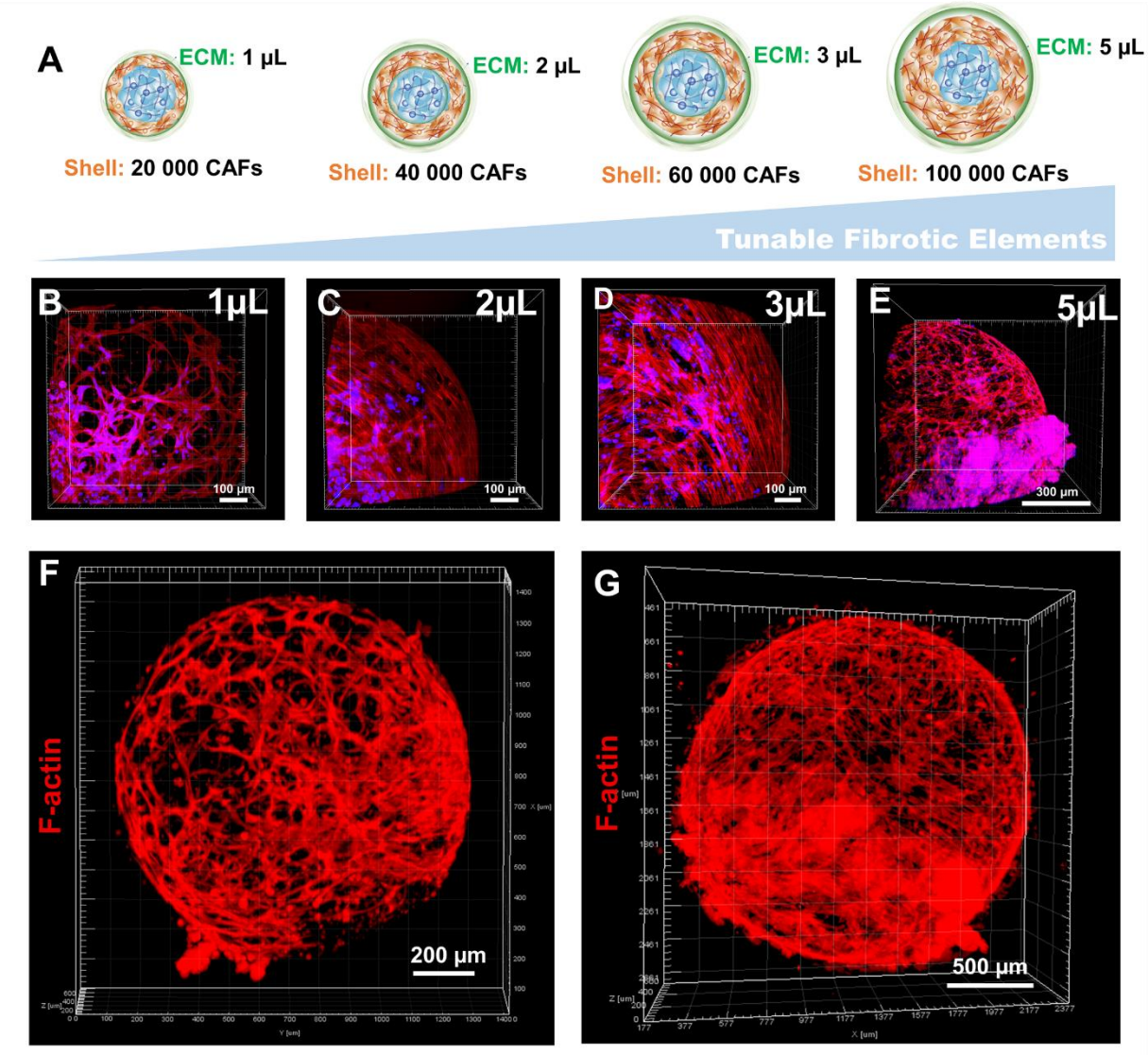

Figure 5. Cancer-on-a-bead living units with differential stromal elements modulation. Analysis via high resolution 3D confocal microscopy. (A-E) Representative 3D sections of

cancer-on-a-bead living units comprising cancer cells surrounded by the stromal CAFs compartment, at day 7 of culture. (F-G) 3D reconstruction of cancer-on-a-bead platforms comprising GelMA/HAMA ECM-mimetic hydrogel compartment laden with CAFs, outer shell of 1µL and 5µL, respectively. Tumor core compartment: 1 µL tumor-ECM mimetic hydrogel, $1x10^3$ PANC-1 cells – constant cell density; Stromal shell: 1 to 5µL, comprising different CAFs cell densities enabling the establishment of PDAC models with variable fibrotic states. Red channel: F-actin. Blue channel: DAPI.

2.6. 3D models biomolecular signature

Human PDAC progression is characterized by complex paracrine and autocrine signaling between tumor and stromal cells, being such complex crosstalk involved in disease progression, resistance, and dissemination to healthy tissues.[51] To further characterize pancreatic cancer-on-a-bead living units potential for emulating the *in vivo* scenario, we characterized the secretion of key biomolecular mediators recognized to be involved in tumor-stroma interplay. As shown in **Figure 6**, both heterotypic PDAC models (i.e., STAMS and cancer-on-a-bead living units) revealed a significantly increased TGF-β expression when compared to monotypic PANC-1 spheroids, revealing the importance of including CAFs in 3D PDAC models to better recapitulate the hallmarks of its microenvironment. Likewise, tumor-stroma 3D cancer-on-a-bead units exhibited up to 1.2-fold higher TGF-β levels than their stratified ECM-free counterparts, evidencing the importance of including cancer cells and CAFs in biomimetic ECM hydrogels (**Figure 6**). The expression of this biomarker is particularly valuable to observe in an *in vitro* setting since TGF-β levels are correlated with pancreatic stellate cells (PSCs) activation, *de novo* ECM deposition, and therapeutics resistance.[52,53] TGF-β may also stimulate epithelial-to-mesenchymal transition (EMT) and resistance to therapeutics resistance through upregulation of TGF-β/VAV1 axis, being an important soluble factor of PDAC TME. [54] In this sense, the established tumor-stroma 3D cancer-on-a-bead units better resemble the native TME owing to the increased secretion of this crucial factor.

Other CAFs activation, invasion and resistance associated factors were also analyzed. In line with this, FGF-2 and PDGF secretion was considerably higher in stratified units when compared to monotypic or heterotypic 3D models (i.e., 3D spheroids, STAMS models, **Figure 6 C, D**). Interestingly, IL-1β secretion was exclusively verified in 3D heterotypic models and a relatively higher expression was obtained in 3D tumor-stroma core-shell units, highlighting the influence of ECM and CAFs spatial, in the acquisition of a more resistant phenotype (**Figure 6 E**). Such possibility was then further evaluated in anti-cancer drug screening assays performed with a standard-of-care chemotherapeutic.

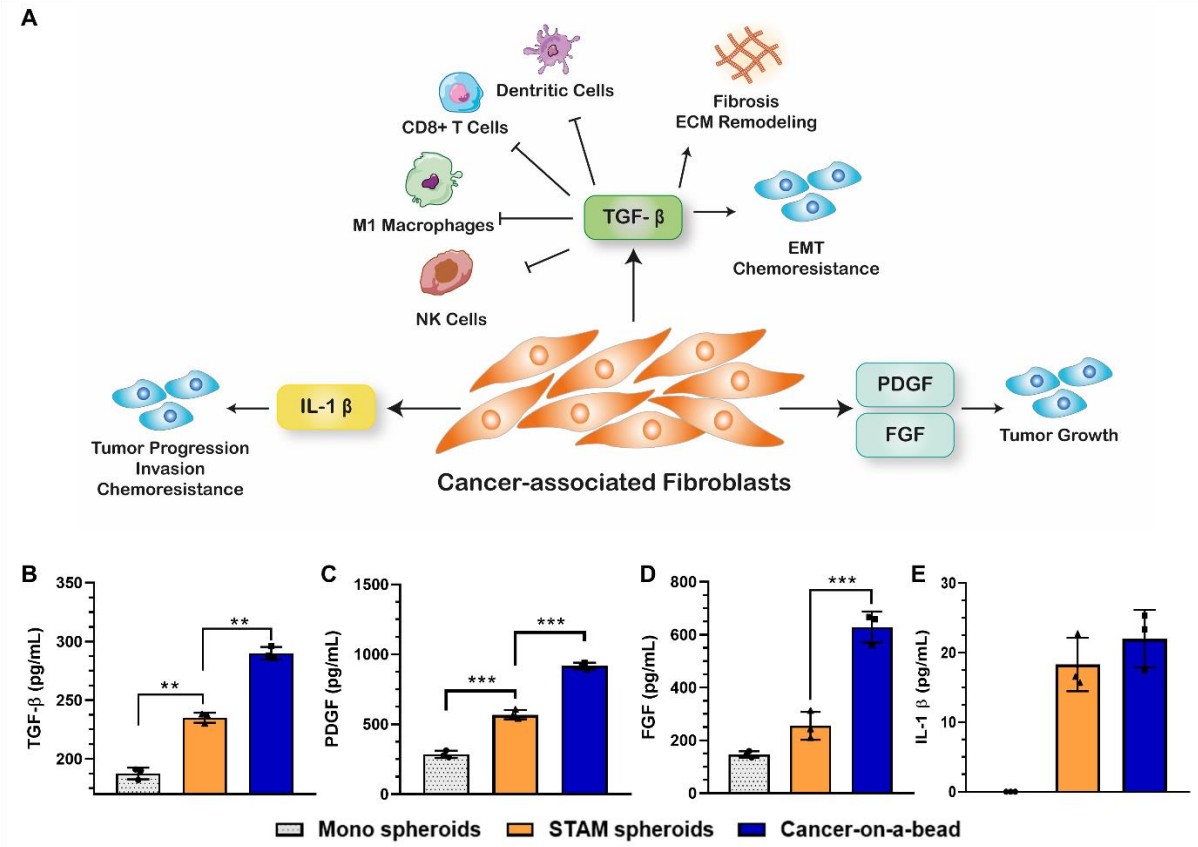

Figure 6. Secretion of pro-tumoral factors by different 3D PDAC models. (A) Schematics of the signaling and key regulatory mediators expressed by CAFs involved in the paracrine signaling between pancreatic cancer cells and CAFs. ELISA-based quantification of (B) TGF-β1, (C) PDGF, (D) FGF-2 and (E) IL-1β, in 3D PDAC platforms culture medium, during 14 days of culture. Data is presented as mean ± s.d., *n*=3; *p<0.05, **<0.01, ***<0.001.

2.7. *In vitro* Drug Screening

The PDAC desmoplastic, stroma-rich tumor microenvironment has been recognized as a major contributor for cancer resistance. To evaluate how cancer-on-a-bead units bioarchitecture and fibrotic stroma cellular elements inclusion influence drug performance analysis we administered Gemcitabine, a clinically validated chemotherapeutic treatment for PDAC. The three different PDAC models were incubated with different concentrations of this chemotherapeutic for 48 h (**Figure 7 and Figure S4**). After incubation, heterotypic PDAC models exhibited a significant resistance in comparison to the monotypic platform, indicating the strong influence of CAFs and bioarchitecture in tumor resistance. The stratified 3D STAMS and cancer-on-a-bead units exhibited a IC_{50} that was 1.5-fold and 1.8-fold higher than that of monotypic spheroids, respectively (**Figure 7 B,C**). Interestingly, 3D cancer-on-a-bead microtumors were 1.16-fold more resistant than STAMS model, also highlighting the importance of including compartmentalized ECM biomimetic components in preclinical tumor

models. Such results have been also corroborated by *in vivo* and *in vitro* studies that evidence the role of PDAC stroma barrier in anti-cancer drug resistance. The performed analysis of soluble tumor mediator factors may sustain these outcomes since TGF-β1 is recognized to be involved in Gemcitabine drug resistance and was significantly higher in the tumor-stroma 3D cancer-on-a-bead models. Additionally, IL-1β that has been associated with poor patients' outcomes and resistance phenotypes exhibited increased secretion in the advanced core-shell bead.[55,56]

To further investigate the physical role of ECM operating as a physical barrier to drug administration cancer-on-a-bead living units were engineered without stromal cells in the shell compartment – herein termed as monotypic cancer-on-a-bead models (**Figure S4**). The monotypic core-shell hydrogel model exhibited a higher drug resistance than the monotypic spheroid. Such evidence the key importance of recapitulating *in vitro* the presence of PDAC ECM-elements, as found *in vivo*. Additionally, monotypic platforms exhibited increased susceptibility to Gemcitabine than the fully assembled tumor-stroma 3D cancer-on-a-bead living units, suggesting the crucial role of CAFs in anti-cancer drug resistance and the importance of including these key stromal elements in PDAC preclinical models. Representative Live/Dead bioimaging further highlighted monotypic spheroids susceptibility to Gemcitabine. **(Figure 7D).**

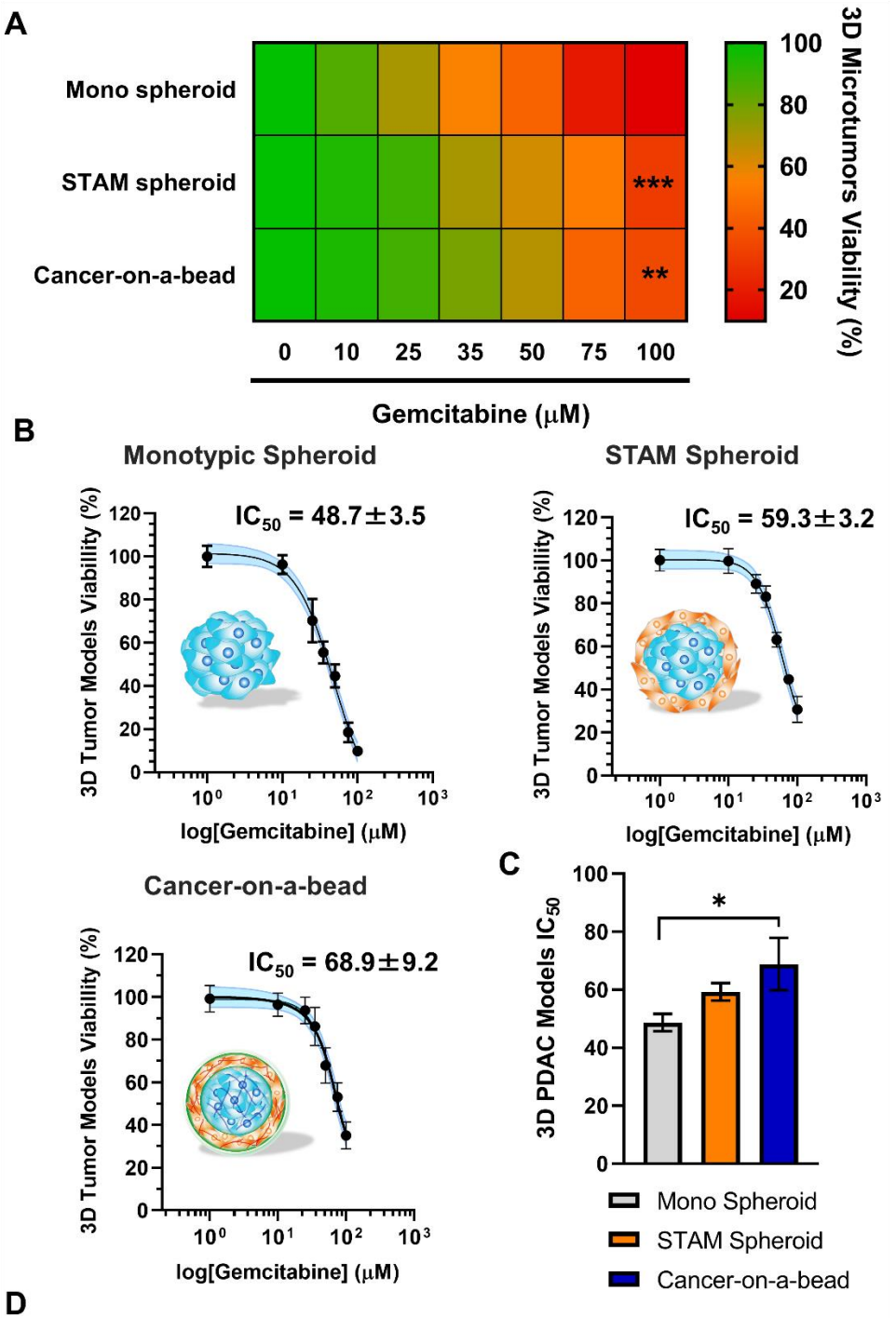
A
Mono spheroid
STAM spheroid
Cancer-on-a-bead
***
**
0 10 25 35 50 75 100
Gemcitabine (μM)
100 80 60 40 20
3D Microtumors Viability (%)
B
Monotypic Spheroid
IC50 = 48.7±3.5
3D Tumor Models Viability (%)
log[Gemcitabine] (μM)
STAM Spheroid
IC50 = 59.3±3.2
Cancer-on-a-bead
IC50 = 68.9±9.2
C
3D PDAC Models IC50
*
Mono Spheroid
STAM Spheroid
Cancer-on-a-bead
D
Monotypic spheroid
STAM spheroid
Cancer-on-a-bead
Non-treated
100 μM
D1
D2
D3
D4
D5
D6
PI
Calcein – AM

404

Figure 7. Susceptibility of 3D PDAC models to the standard-of-care Gemcitabine chemotherapeutic. Tumor-stroma 3D cancer-on-a-bead models exhibit higher resistance than their free monotypic and stratified heterotypic spheroids devoid of ECM. (A) Heat-map representation of Gemcitabine induced cell death to the tested concentrations. Data is presented as mean ± s.d. (n = 5), *p<0.05 (in comparison to STAM spheroid), ** p<0.01 (in comparison to monotypic spheroid). (B) IC_{50} calculation for the established PDAC models. (C) Statistical analysis of *in vitro* 3D models IC_{50} values. Blue area represents the area between the upper and lower error bands for the interpolation curve. (D) Representative live/dead micrographs of Monotypic spheroids, STAMS, and cancer-on-a-bead models incubated with Gemcitabine (100 µm). Non-treated microtumors were used as controls. A clear disruption of 3D monotypic spheroids mass was observed after gemcitabine treatment. Scale bar= 250 µm. Data is presented as mean ± s.d. (n = 5), *p<0.05, ** p<0.01, ***p<0.001.

Overall, *in vitro* drug screening further highlighted the importance of not only including stromal cells, but also the importance of introducing specific ECM-mimetic hydrogels with a programmed stratification.

3. Conclusions

Capturing PDAC complexity by patterning cancer-stroma cells and ECM-mimetic components in a relevant mode that recapitulates native tumor bioarchitecture and composition is highly advantageous to improve pre-clinical models' robustness and predictive potential. Herein, we employed superhydrophobic surfaces for bioengineering a biomimetic core-shell tumor-stroma PDAC model – so termed 3D pancreatic cancer-on-a-bead living units - that not only comprise key stromal cells (i.e., CAFs) in a juxtatumoral position to cancer cells, but also that include stroma and tumor ECM-mimetic hydrogel compartments. ECM components are spatially compartmentalized in a mode that better mimics their biological arrangement in the human tumor niche, as an attempt to recapitulate the *in vivo* tumor bioarchitecture. In such assemblies, cancer cells closely interact with the supporting matrix and the surrounding stroma compartment specifically designed to mimic differential cellular-ECM organization. Importantly, cancer-on-a-bead living units exhibited increased biomolecular markers secretion and drug resistance when compared to their monotypic and heterotypic scaffold-free counterparts, emphasizing the importance of including ECM components and pancreatic cancer-stroma cellular elements similarly to the native environment. Herein, we selected GelMA and hyaluronan to mimic native ECM components as these have been widely reported for *in vitro* tumor models development. Nevertheless, owing to superhydrophobic platforms versatility we envision that collagen and decellularized extracellular matrix biomaterials can also be employed in pancreatic cancer models generation. Furthermore, these living units may

unlock the possibility to specifically evaluate chemotherapeutics individualized effect on cancer cells or stromal elements, an important aspect to be explored in the future.

Stratified living hydrogels also enabled a precise programming of both ECM and fibrotic elements on-demand and in a highly cost-effective and reproducible mode completely devoid of organic solvents, generally required for producing spherically structured hydrogel beads in other technologies such as those based on microfluidics. The possibility to assemble core/shell compartments with other ECM-biomimetic hydrogels while varying mechanical properties, or the culture of other key stromal cells players (i.e., immune cells) may also contribute to study cancer-immune system interactions or anti-cancer drug delivery in the future.

The ease of assembly, the low-cost, the reproducible features, as well as the possibility to evaluate cellular response by standard imaging methodologies, renders stratified cancer-on-a-bead living units highly valuable platforms for inclusion in static and dynamic high-throughput screening systems (i.e., bioreactors, microphysiological systems, etc.), while benefiting from an increased biomimicry level. Overall, the universality of the described cancer-on-a-bead living units may open new avenues for bioengineering evermore physiomimetic tumor models with a precise control over size/shape, number/type of cells, and nature of the ECM-mimetic biomaterials that are included, broadening cancer living units' applicability in the modelling of other neoplasias.

4. Experimental Section

Materials: Ultra-Low adhesion (ULA) U-bottom 96-well plates (Corning™,7007), Fetal Bovine Serum (FBS, E.U. approved, South America origin), Dulbecco's Modified Eagle Medium-High Glucose (DMEM-HG), phosphate buffered saline, without Ca^{2+} and Mg^{2+} (D-PBS, pH = 7.4), Antibiotic-Antimycotic (ATB, Gibco® - 10,000 U/mL of penicillin, 10,000 µg/mL of streptomycin, and 25 µg/mL of Amphotericin B), 4,6-diamidino-2-phenylindole (DAPI), Calcein-AM, Propidium Iodide (PI), Trinitrobenzene Sulfonic Acid (TNBS), FGF-2 basic ELISA kit (KHG0022), DiD and DiO were purchased from Thermofisher Scientific (Alfagene, Carcavelos, Portugal). Trypsin-EDTA detaching solution, gelatin form porcine skin type A, and Hyaluronic acid (MW: ~1.5-1.8 x 10^6 Da) were obtained from Laborspirit (Merck-Sigma, Portugal). WX 2100™ was purchased from Cytonix (Cytonix LLC, MD, US). MSC-GRO™ Low serum, complete media was obtained from Neuromics (Neuromics, Inc, MN, USA). CellTiter-Glo 3D® Cell Viability Assay was obtained from VWR (VWR Portugal, Promega Madison, USA). Human TGF-β1 (ab108912), PDGF-BB (ab184860), IL-1β

(ab46052) ELISA kits and Phalloidin-iFluor 594 (ab176757), were purchased from Abcam, (Abcam plc, Cambridge, UK).

Gelatin methacrylate synthesis: Gelatin methacrylate (GelMA) was synthesized based on the a previously described methodology.[13] In brief, gelatin was dissolved in a PBS solution (pH 7.4), at 50 °C, to yield a 10 % (w/v) working solution. Thereafter, 0.6 g of methacrylic anhydride/gram of gelatin was dropwise added under mild magnetic stirring. The reaction was then allowed to proceed for 5 h, at 50 ºC with constant magnetic stirring. After this period the solution was centrifuged (3 min, 3500 g, at room temperature (RT)) to promote phase separation between gelatin and non-reacted methacrylic anhydride. The remaining gelatin methacrylate (GelMA) was then diluted and dialyzed (MWCO 6-8 kDa), at 50 °C. The purified GelMA was recovered by freeze drying (-86 °C, Telstar LyoQuest) for 6 days, in the dark. The obtained degree of substitution was D.S.: 85.2 ± 1.2 %, as determined by the TNBS assay.[13]

Hyaluronic acid methacrylate synthesis: Methacrylated hyaluronic acid (HAMA) was synthesized by reacting hyaluronic acid (MW: ~1.5-1.8 x 10^6 Da) with glycidyl methacrylate under alkaline conditions as previously described with minor modifications.[57] In brief, hyaluronic acid (HA, 2.0 g), was dissolved in double deionized distilled and filtered ultrapure water (Milli-Q® water, 200 mL), under magnetic stirring, at room temperature (RT), to yield a 1% w/v aqueous solution. Afterwards, glycidyl methacrylate (35.5 mL) and triethylamine (25.3 mL) were drop-wise added to N,N-dimethylformamide (DMF), in a Schott Flask under magnetic stirring. Afterwards, the organic DMF phase was added to HA aqueous phase, and the reaction occurred for 72 h, protected from light. The modified polymer solution was then carefully transferred to a dialysis tubing (MWCO: 6–8 kDa), and dialyzed for 5 days, at RT, by using double distilled deionized water as dialysant. The purified polymer was then freeze-dried (-86 ºC), for 7 days, in the dark. HA degree of methacrylation was determined through ^{1}H NMR spectroscopy as described in the literature.[58] The obtained degree of substitution was D.S.: 19.4 ± 1.8 %.

Superhydrophobic platforms fabrication: The production of polystyrene superhydrophobic surfaces was performed as previously described.[57] In brief, circular polystyrene 90 mm petri dish plates were spray coated with a U.V. resistant FluoroThane-MW reagent (WX 2100™) and left to dry overnight in a chemical safety fume hood. In the following day, the petri dish surface was washed with 99% ethanol and oven dried at 37 °C for 48 h.

In-air generation ECM-mimetic hydrogel units: Stratified 3D core-shell hydrogel beads were produced via a sequential two-stage procedure by using a mechanical electronic repeater pipette (Eppendorf® M4, Eppendorf, VWR) and polystyrene superhydrophobic surfaces

(supplementary **Video S1**). GelMA-based core units and GelMA:HAMA core-shell units of different sizes were produced by dispensing different volumes of hydrogel precursor solution into superhydrophobic surfaces (**Figure 1**). Initially, for assembling the core template, GelMA 5% (w/v, pre-heated at 40ºC) was loaded into 0.1 mL plastic tips (Combitip advanced® positive displacement, Eppendorf, VWR), mechanically dispensed over the superhydrophobic surface and then photocrosslinked for 80 secs by using lithium phenyl-2,4,6-trimethylbenzoylphosphinate (LAP) (0.5 % w/v) as a photoinitiator and a LED curing system (UniLight 406 nm, Sarspec, 9.25 mW.cm^{-2}). To generate tunable core-shell units a two-stage fabrication strategy was optimized. In a first stage: a GelMA core template bead of 1 µL was dispensed onto the superhydrophobic surface and photocrosslinked for 40 secs. In a second stage: a pre-heated (40 ºC) GelMA 5%-HAMA 1% (w/v) formulation was used for generating the shell compartments of different volumes (1 - 5 µL). For this purpose, hydrogel precursor solutions were loaded into 0.1 mL plastic tips (Combitip advanced® positive displacement, Eppendorf, VWR), and were mechanically dispensed over the core bead to generate the stratified system. Core-shell platforms were then photocrosslinked for 40 secs, as above described. Through this sequential approach, different compartments with dissimilar hydrogel composition, cell density and size were easily assembled in-air. This strategy is completely devoid of additional organic/oil solvents generally required for other emulsion/on-chip based technologies and enables a precise control over dispensed biomaterials.

Hydrogel unit beads size, concentricity and morphological analysis were performed by optical imaging. For size evaluation different hydrogels were imaged by using a Canon EOS 1200d DLSR camera equipped with a macro lens 60mm. Image analysis was performed in an open-source software ImageJ (Fiji package, NIH, USA). Core-shell units concentricity was determined as previously described and according to the following equation 1:

$$Concentricity = \left(1 - \frac{d_{offset}}{D_{avg}}\right) \quad (1)$$

, where d_{offset} is the distance between the center of the shell bead and the center of the core bead, and D_{avg} is the average core-shell bead diameter.[59] The s.d. associated to each bead analysis results from at least three technical measurement replicates for each single hydrogel beads. A total of 12 hydrogels were evaluated to determine average concentricity.

Cell Culture: Human pancreatic cancer cells (PANC-1, ATCC® CRL-1469™) were cultured in Dulbecco's modified Eagle's medium high glucose (DMEM-HG) supplemented with sodium bicarbonate (3.7 g.L^{-1}), 10% heat-inactivated fetal bovine serum (FBS), and 1%

antibiotic/antimycotic. Human Pancreatic CAF-Stellate Cells (CAF08, Neuromics, USA) were cultured in MSC-GRO™ Low serum, Complete Media, supplemented with 1 % antibiotic/antimycotic, according to manufacturer's instructions. Both cancer and stromal cells were cultured in cell culture treated T-flasks, and maintained under 5 % CO_2 atmosphere, at 37 °C. The medium was replaced every 2-3 days.

Generation of Pancreatic cancer-on-a-bead living models: The generation of tumor-stroma 3D PDAC cancer-on-a-bead models comprising living cells was performed by using superhydrophobic surfaces and visible LED light- mediated photocrosslinking. For establishing 3D tumor-stroma cancer-on-a-bead platforms, in the first stage, tumor core beads (1 µL) combining PANC-1 laden in a GelMA matrix were dispensed over the superhydrophobic surface and photocrosslinked (40 sec, LED 406 nm, 9.25 $mW.cm^{-2}$). In the second stage, stroma shell beads (2 µL) combining CAFs laden in a GelMA-HAMA matrix were dispensed above the core bead to generate the stratified system. The core-shell platform was crosslinked as above mentioned and the obtained tumor-stroma units were transferred to 96-well round bottom ultra-low adhesion (ULA) plates for *in vitro* culture and maturation.

In addition, conventional 3D tumor spheroids (controls) were also established in to evidence the importance of including both stromal cells and ECM-mimetic matrices in preclinical pancreatic cancer models. Monotypic spheroids (i.e., comprising cancer cells only), and stratified microenvironment spheroid (STAMS, i.e., comprising cancer cells and CAFs in a core-shell architecture) scaffold-free models were generated by using the liquid overlay technique (LOT). For this, cells were placed in ULA plates that promote cellular self-aggregation into a scaffold-free microtumor. For assembling monotypic PANC-1 spheroids, a cellular suspension (i.e., $1x10^4$ cells per well) was prepared and seeded into 96-well ULA plates in order to generate 3D spheroids via LOT. For generating heterotypic 3D STAMS, a two-step strategy was established as previously described.[5] In the first stage of assembly, a 3D spheroid core comprising PANC-1 cells was placed in *in vitro* culture. At day 6 of maturation, a suspension of human pancreatic stellate CAFs was seeded in the wells containing a tumor core spheroid to establish the stratified 3D heterotypic model (devoid of ECM components).

For all tumor-stroma models, CAFs population represented 80% of the tumor mass in order to better recapitulate the stromal occupancy ratio found in the *in vivo* scenario.[60] All the generated 3D PDAC models were maintained under 5% CO_2 atmosphere at 37 °C, and the culture medium was replaced every 3 days. 3D *in vitro* PDAC models morphometric parameters including size and circularity were analyzed at day 3, 7 and 14 of culture, via optical contrast microscopy by using an inverted microscope (Zeiss Primovert, Carl Zeiss, Germany). Image

analysis was performed in open-source software ImageJ (Fiji package, NIH, USA) by employing a supervised algorithm developed by Ivanov and co-workers.[61]

Cell Tracking Analysis: To track volumetric cellular distribution in the different monotypic, heterotypic and cancer-on-a-bead PDAC models, cancer cells (PANC-1) and stromal elements (CAFs) were incubated with long term cell tracking lipophilic dyes, namely DiO and DiD, respectively, prior to 3D tumor models fabrication. In brief, cells were incubated with the suitable dye (2 µM per $1x10^6$ cells), at 37 °C, for 15 min, at RT. Afterwards, 3D tumor models were generated as before described. Labelled tumor models were imaged in a Axio Imager M2 widefield fluorescence microscope equipped with a 3MPix monochromatic camera and a Plan-Neofluar 5x/0.16 M27 objective (Carl Zeiss Microscopy, Germany). Fluorescence micrographs were acquired and analyzed in Zeiss Zen Software (ZEN 2019, SP3.0).

Cell morphological analysis: Cell morphology and cytoskeletal spatial arrangement analysis was performed through DAPI/Phalloidin staining at day 1 and 7 of culture. Briefly, tumor-stroma 3D PDAC cancer-on-a-bead models were washed with PBS and fixed in a solution of 4% (v/v) formaldehyde for 24 h. After washing three times with dPBS, samples were permeabilized with 0.5% (v/v) Triton X-100 for 20 min. For F-actin staining, tumor-stroma 3D PDAC cancer-on-a-bead models were incubated with Flash Phalloidin™ Red 594 (1:40 (v/v) in dPBS) at RT for 48 h and then washed with dPBS. Afterwards, a DAPI solution (1:1000 (v/v)) was used to incubate the PDAC platforms during 30 min, at RT. After washes with PBS three times, the 3D models were observed under a scanning confocal microscope (LSM 880 Airyscan, Carl Zeiss, Germany).

3D models cell viability analysis: After 3, 7 and 14 days of culture, a Live/Dead cell assay was performed for viability assessment. Briefly, 3D tumor spheroids were incubated with Calcein AM and propidium iodide (PI) in PBS at standard culture conditions (5% CO_2 at 37 °C), for 30 min. After washing with PBS, the 3D tumor models were observed under a widefield fluorescence microscope (Fluorescence Microscope Zeiss, Axio Imager 2, Carl Zeiss, Germany). Furthermore, the cell proliferation of core-shell tumor-stroma PDAC beads was accessed by ATP quantification using the CellTiter-Glo 3D® Cell Viability Assay. CellTiter-Glo assay was performed in accordance with the manufacturer instructions. Luminescence was measured in 96-well flat-bottom white plates by using a multi-modal Synergy HTX microplate reader (BioTek Instruments, Winooski, USA).

3D Models biomolecular signatures: The quantification of soluble biomolecular markers secreted by the different 3D PDAC models including: (i) human TGF-β1, (ii) PDGF-BB, (iii)

FGF-2 and (iv) IL-1β was performed by ELISA. In brief, at pre-determined time points (7 and 14 days) the culture medium (n=3) of each condition was retrieved and stored at -80 ºC. Human PDAC biomolecular markers quantification was performed by sandwich ELISA according to manufacturer's instructions. Absorbance was determined by using a multi-modal Synergy HTX microplate reader (BioTek Instruments, USA).

In vitro drug screening: 3D tumor models' response to anti-cancer chemotherapeutics was evaluated following incubation with the standard-of-care Gemcitabine. In brief, the different PDAC 3D models were incubated with a series of concentrations after 14 days of culture (0-100 µM). In each assay, 3D PDAC tumors were incubated during 48 h with Gemcitabine. Anti-cancer drug cytotoxicity was assessed after 48 h of dugs administration by ATP quantification using the CellTiter-Glo 3D® Cell Viability Assay, in accordance with the manufacturer instructions. Briefly, CellTiter-Glo reagent was added at a 1:1 ratio in cell culture medium, the samples were then vigorously mixed for 5 min in a horizontal plate shaker, following incubation for 25 min, at RT, in the dark. Luminescence was measured in 96-well flat-bottom opaque white plates by using a multi-modal Synergy HTX microplate reader (BioTek Instruments, USA).

Statistical Analysis: Statistical analysis was performed in GraphPad Prism 9 Software (Prism 9™, trial version). One-way analysis of variance (One-way ANOVA) with Tukey's multiple comparisons was generally used for data analysis. A value of $p < 0.05$ was considered to be statistically significant.

Supporting Information

Supporting Information is available from the Wiley Online Library or from the author.

Acknowledgements

This work was developed within the scope of the project CICECO-Aveiro Institute of Materials, UIDB/50011/2020 & UIDP/50011/2020, financed by national funds through the Portuguese Foundation for Science and Technology/MCTES. This work was also supported by the Programa Operacional Competitividade e Internacionalização (POCI), in the component FEDER, and by national funds (OE) through FCT/MCTES, in the scope of project PANGEIA (PTDC/BTM-SAL/30503/2017). The authors acknowledge the financial support by the Portuguese Foundation for Science and Technology (FCT) through a Doctoral Grant (DFA/BD/7692/2020, M.V.M.). The authors also acknowledge the financial support by the Portuguese Foundation for Science and Technology (FCT) through a Junior Researcher contract (CEEC/1048/2019, V.M.G.).

Received: ((will be filled in by the editorial staff))
Revised: ((will be filled in by the editorial staff))
Published online: ((will be filled in by the editorial staff))

References

[1] B. Blanco-Fernandez, V. M. Gaspar, E. Engel, J. F. Mano, *Adv. Sci.* **2021**, *8*, 2003129.

[2] E. L. S. Fong, D. A. Harrington, M. C. Farach-Carson, H. Yu, *Biomaterials* **2016**, *108*, 197.

[3] C. Il Hwang, S. F. Boj, H. Clevers, D. A. Tuveson, *J. Pathol.* **2016**, *238*, 197.

[4] J. Radhakrishnan, S. Varadaraj, S. K. Dash, A. Sharma, R. S. Verma, *Drug Discov. Today* **2020**, *25*, 879.

[5] M. V. Monteiro, V. M. Gaspar, L. Mendes, I. F. Duarte, J. F. Mano, *Small Methods* **2021**, *5*, 2001207.

[6] M. Duchamp, T. Liu, A. M. van Genderen, V. Kappings, R. Oklu, L. W. Ellisen, Y. S. Zhang, *Biotechnol. J.* **2019**, *14*, 1.

[7] X. Cao, R. Ashfaq, F. Cheng, S. Maharjan, J. Li, G. Ying, S. Hassan, H. Xiao, K. Yue, Y. S. Zhang, *Adv. Funct. Mater.* **2019**, *29*, 1807173.

[8] M. A. Heinrich, R. Bansal, T. Lammers, Y. S. Zhang, R. Michel Schiffelers, J. Prakash, *Adv. Mater.* **2019**, *31*, 1806590.

[9] J. Li, C. Parra-Cantu, Z. Wang, Y. S. Zhang, *Trends in Cancer* **2020**, *6*, 745.

[10] S. R. Nelson, C. Zhang, S. Roche, F. O'Neill, N. Swan, Y. Luo, A. M. Larkin, J. Crown, N. Walsh, *Sci. Rep.* **2020**, *10*, 1.

[11] M. V Monteiro, Y. S. Zhang, V. M. Gaspar, J. F. Mano, *Trends Biotechnol.* **2021**.

[12] L. A. Baker, H. Tiriac, H. Clevers, D. A. Tuveson, *Trends in Cancer* **2016**, *2*, 176.

[13] M. V. Monteiro, V. M. Gaspar, L. P. Ferreira, J. F. Mano, *Biomater. Sci.* **2020**, *8*, 1855.

[14] S. L. Wood, M. Pernemalm, P. A. Crosbie, A. D. Whetton, *Cancer Treat. Rev.* **2014**, *40*, 558.

[15] T. Risom, D. R. Glass, C. C. Liu, B. Rivero-Gutiérrez, A. Baranski, E. F. McCaffrey, N. F. Greenwald, A. Kagel, S. H. Strand, S. Varma, et al., *bioRxiv* **2021**.

[16] H. G. Yi, Y. H. Jeong, Y. Kim, Y. J. Choi, H. E. Moon, S. H. Park, K. S. Kang, M. Bae, J. Jang, H. Youn, et al., *Nat. Biomed. Eng.* **2019**, *3*, 509.

[17] K. P. Olive, *Clin. Cancer Res.* **2015**, *21*, 3366.

[18] P. Dauer, A. Nomura, A. Saluja, S. Banerjee, *Pancreatology* **2017**, *17*, 7.

[19] F. Di Maggio, K. H. El-Shakankery, *Pancreas* **2020**, *49*, 313.

[20] J. Alcaraz, J. Lluís, L. Millares, I. Luis, F. J. Fernández-porras, A. Martínez-romero, N. Diaz-valdivia, J. Sánchez, D. Cos, R. Rami-porta, et al., *Lung Cancer* **2020**, *135*, 151.

[21] W. J. Ho, E. M. Jaffee, L. Zheng, *Nat. Rev. Clin. Oncol.* **2020**, *17*, 527.

[22] E. Tomás-Bort, M. Kieler, S. Sharma, J. B. Candido, D. Loessner, *Theranostics* **2020**, *10*, 5074.

[23] R. A. Høglund, A. A. Maghazachi, **2014**, *4*, 27.

[24] M. A. Heinrich, A. M. R. H. Mostafa, J. P. Morton, L. J. A. C. Hawinkels, J. Prakash, *Adv. Drug Deliv. Rev.* **2021**, *174*, 265.

[25] A. Santi, F. G. Kugeratski, S. Zanivan, *Proteomics* **2017**, *18*, e1700167.

[26] C. Tian, K. R. Clauser, D. Öhlund, S. Rickelt, Y. Huang, M. Gupta, D. R. Mani, S. A. Carr, D. A. Tuveson, R. O. Hynes, *Proc. Natl. Acad. Sci.* **2019**, *116*, 201908626.

[27] F. M. Galogahi, Y. Zhu, H. An, N. T. Nguyen, *J. Sci. Adv. Mater. Devices* **2020**, *5*, 417.

[28] M. P. A. Lim, W. L. Lee, E. Widjaja, S. C. J. Loo, *Biomater. Sci.* **2013**, *1*, 486.

[29] L. Yu, C. Ni, S. M. Grist, C. Bayly, K. C. Cheung, *Biomed. Microdevices* **2015**, *17*, 1.

[30] A. M. S. Costa, J. F. Mano, *J. Am. Chem. Soc.* **2017**, *139*, 1057.

[31] A. Rascón-Chu, J. A. Díaz-Baca, E. Carvajal-Millan, E. Pérez-López, A. T. Hotchkiss, H. González-Ríos, R. Balandrán-Quintana, A. C. Campa-Mada, *Polymers.* **2018**, *10*, 108.

[32] M. Khanmohammadi, V. Zolfagharzadeh, Z. Bagher, H. Soltani, J. Ai, *Biomed. Phys. Eng.* **2019**, 1.

[33] A. M. S. Costa, N. V. Dencheva, S. G. Caridade, Z. Z. Denchev, J. F. Mano, *Adv. Mater. Interfaces* **2016**, *3*, 1600074.

[34] C. Schlaich, Y. Fan, P. Dey, J. Cui, Q. Wei, R. Haag, X. Deng, *Adv. Mater. Interfaces* **2018**, *5*, 1701536.

[35] S. Pandol, M. Edderkaoui, I. Gukovsky, A. Lugea, A. Gukovskaya, *Clin. Gastroenterol. Hepatol.* **2009**, *7*, 1.

[36] C. J. Whatcott, C. H. Diep, P. Jiang, A. Watanabe, J. Lobello, C. Sima, G. Hostetter, H. M. Shepard, D. D. Von Hoff, H. Han, *Clin. Cancer Res.* **2015**, *21*, 3561.

[37] T. Seufferlein, M. Ducreux, M. Hidalgo, G. Prager, E. Van Cutsem, *Eur. Oncol. Haematol.* **2018**, *14*, 40.

[38] N. Sato, N. Maehara, M. Goggins, *Cancer Res.* **2004**, *64*, 6950.

[39] N. Sato, S. Kohi, K. Hirata, M. Goggins, *Cancer Sci.* **2016**, *107*, 569.

[40] S. Dangi-Garimella, S. B. Krantz, M. R. Barron, M. A. Shields, M. J. Heiferman, P. J. Grippo, D. J. Bentrem, H. G. Munshi, *Cancer Res.* **2011**, *71*, 1019.

[41] A. D. Arya, P. M. Hallur, A. G. Karkisaval, A. Gudipati, S. Rajendiran, V. Dhavale, B. Ramachandran, A. Jayaprakash, N. Gundiah, A. Chaubey, *ACS Appl. Mater. Interfaces* **2016**, *8*, 22005.

[42] C. Ricci, C. Mota, S. Moscato, D. D'Alessandro, S. Ugel, S. Sartoris, V. Bronte, U. Boggi, D. Campani, N. Funel, et al., *Biomatter* **2014**, *4*, 1.

[43] H. Y. Liu, M. Korc, C. C. Lin, *Biomaterials* **2018**, *160*, 24.

[44] J. Antunes, V. M. Gaspar, L. Ferreira, M. Monteiro, R. Henrique, C. Jerónimo, J. F. Mano, *Acta Biomater.* **2019**, *94*, 392.

[45] J. Yin, M. Yan, Y. Wang, J. Fu, H. Suo, *ACS Appl. Mater. Interfaces* **2018**, *10*, 6849.

[46] D. Loessner, C. Meinert, E. Kaemmerer, L. C. Martine, K. Yue, P. A. Levett, T. J. Klein, F. P. W. Melchels, A. Khademhosseini, D. W. Hutmacher, *Nat. Protoc.* **2016**, *11*, 727.

[47] A. Kiemen, A. M. Braxton, M. P. Grahn, K. S. Han, J. M. Babu, R. Reichel, F. Amoa, S. M. Hong, T. C. Cornish, E. D. Thompson, et al., *bioRxiv* **2020**, 2020.12.08.416909.

[48] I. Yakavets, A. Francois, A. Benoit, J. L. Merlin, L. Bezdetnaya, G. Vogin, *Sci. Rep.* **2020**, *10*, 1.

[49] H. Y. Liu, T. Greene, T. Y. Lin, C. S. Dawes, M. Korc, C. C. Lin, *Acta Biomater.* **2017**, *48*, 258.

[50] M. Löhr, C. Schmidt, J. Ringel, M. Kluth, P. Müller, H. Nizze, R. Jesnowski, *Cancer Res.* **2001**, *61*, 550.

[51] D. Mahadevan, D. D. Von Hoff, *Mol. Cancer Ther.* **2007**, *6*, 1186.

[52] A. Turtoi, D. Musmeci, Y. Wang, B. Dumont, J. Somja, G. Bevilacqua, E. De Pauw, P. Delvenne, V. Castronovo, *J. Proteome Res.* **2011**, *10*, 4302.

[53] Q. Sun, B. Zhang, Q. Hu, Y. Qin, W. Xu, W. Liu, X. Yu, J. Xu, *Theranostics* **2018**, *8*, 5072.

[54] Z. Gu, Y. Du, X. Zhao, C. Wang, *Cancer Lett.* **2021**, *521*, 98.

[55] S. Mitsunaga, M. Ikeda, S. Shimizu, I. Ohno, J. Furuse, M. Inagaki, S. Higashi, H. Kato, K. Terao, *Br. J. Cancer* **2013**, 2063.

[56] S. Müerköster, K. Wegehenkel, A. Arlt, M. Witt, B. Sipos, M. L. Kruse, T. Sebens, G. Klöppel, H. Kalthoff, U. R. Fölsch, et al., *Cancer Res.* **2004**, *64*, 1331.

[57] J. Antunes, V. M. Gaspar, L. Ferreira, M. Monteiro, R. Henrique, C. Jerónimo, J. F. Mano, *Acta Biomater.* **2019**, *94*, 392.

[58] A. Sigen, Q. Xu, P. Mcmichael, Y. Gao, X. Li, X. Wang, *RSC Adv.* **2015**, *5*, 106094.

[59] J. Li, J. Lindley-Start, A. Porch, D. Barrow, *Sci. Rep.* **2017**, *7*, 1.

[60] D. Von Ahrens, T. D. Bhagat, D. Nagrath, A. Maitra, A. Verma, *J. Hematol. Oncol.* **2017**, *10*, 1.

[61] D. P. Ivanov, T. L. Parker, D. A. Walker, C. Alexander, M. B. Ashford, P. R. Gellert, M. C. Garnett, *PLoS One* **2014**, *9*, 1.

M. V. Monteiro, M. Rocha, V. M. Gaspar*, J. F. Mano*

Programmable Living Units for Emulating Pancreatic Tumor-Stroma Interplay

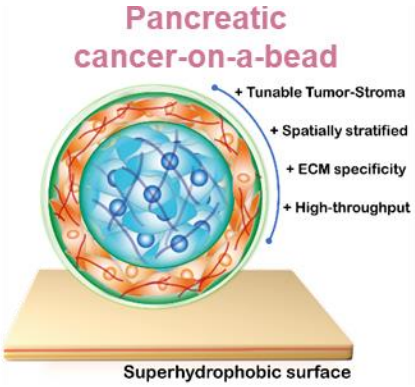

In this study, a methodology using superhydrophobic surfaces is proposed to establish 3D cancer-on-a-bead models. Such stratified living model aims to recapitulate key PDAC features including its unique bioarchitecture and the differential spatially organization of both tumor and stromal components by tunning both cells and ECM compartments independently. The developed technology opens new avenues for the large-scale fabrication of stratified living platforms compatible with high-throughput/high-content imaging analysis.

Supporting Information

Programmable Living Units for Emulating Pancreatic Tumor-Stroma Interplay

Maria V. Monteiro, Marta Rocha, Vítor M. Gaspar, João F. Mano**

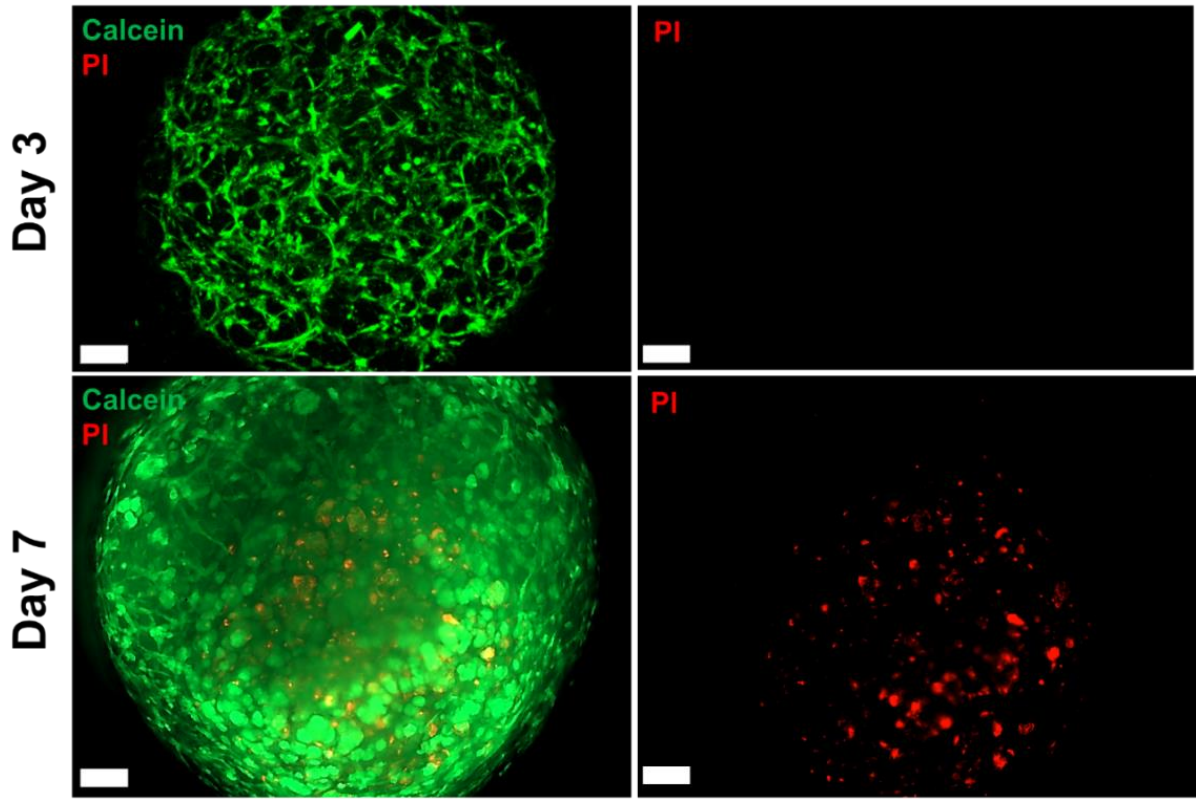

Figure S1. 3D cancer-on-a-bead viability at day 3 and 7 of culture. The shell compartment is comprised by 3 µL and CAFs ($4x10^4$ cells per 1 µL of GelMA:HAMA ECM). Green channel: Calcein-AM, Red channel: PI. Scale bar=200 µm.

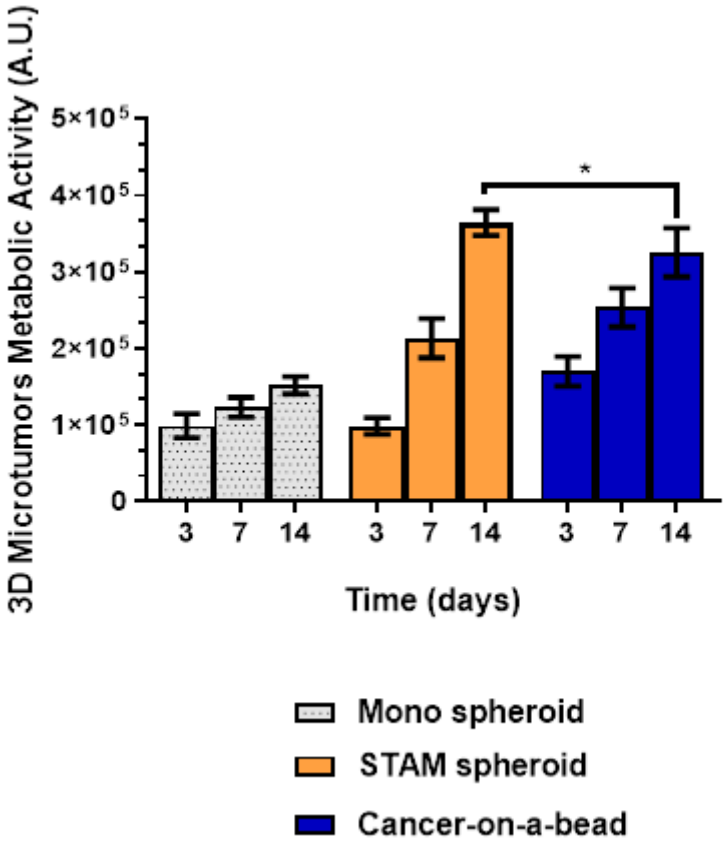

Figure S2. Analysis of different PDAC 3D microtumors models' viability along time. Data is presented as mean ± s.d., *n*=5, *p<0.05.

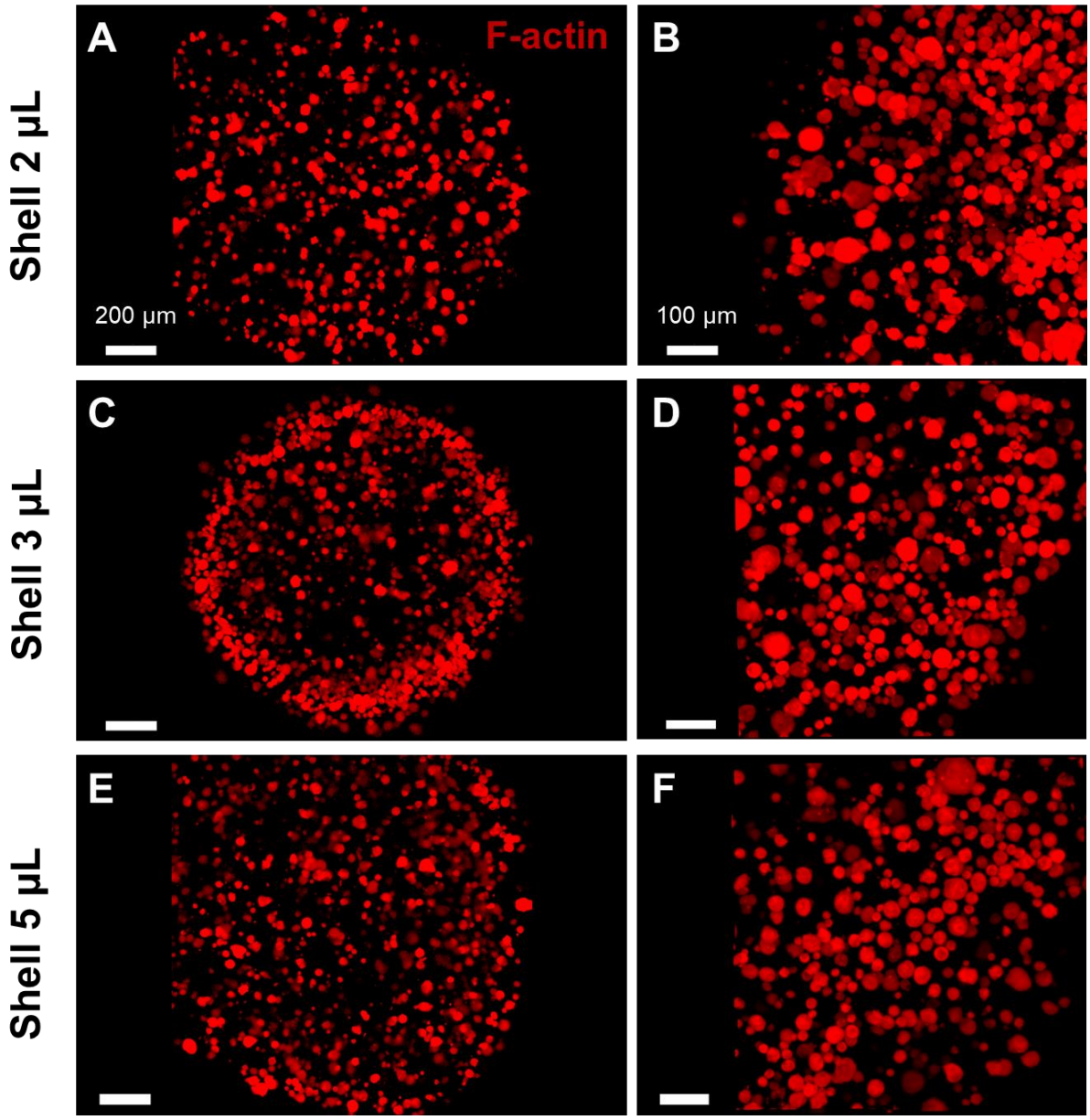

Figure S3. High-resolution confocal bioimaging of actin filaments organization in 3D cancer-on-a-bead units with different shell volume and variable stromal CAFs density (2µL - $4x10^4$ cells; 3µL - $6x10^4$ cells; 5µL - $1x10^5$ cells), at 1 day of culture. At day 1 of culture, CAFs laden in the GelMA:HAMA shell exhibited a rounded shape morphology requiring maturation time to acquire a functional myofibroblast-like fusiform morphology and cell spreading (verified at day 7 of culture). Red channel: F-actin filaments. Scale bar= 200 µm (A, C, E) and scale bar = 100 µm (B, D, F).

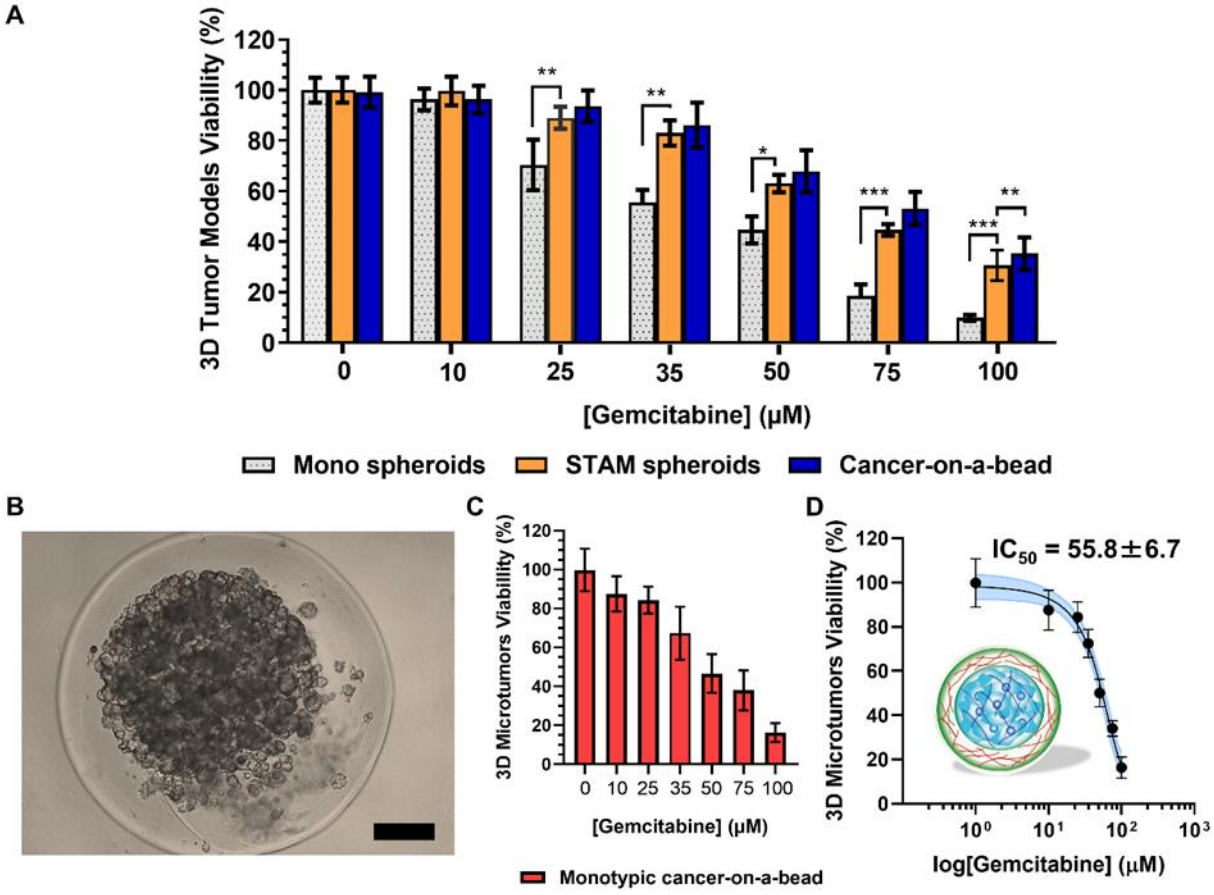

Figure S4. Susceptibility of 3D PDAC models to Gemcitabine chemotherapeutics. (A) Full statistical analysis of Gemcitabine screening in *in vitro* 3D models (i.e., monotypic spheroid, STAMs model, and tumor-stroma cancer-on-a-bead), at day 14 of culture. (B and C) Statistical analysis of monotypic cancer on-a-bead (comprised by cancer cells in the core compartment, without stromal cells in the shell) treated with the different concentrations of Gemcitabine at day 14 of culture. (D) IC_{50} analysis for established monotypic cancer-on-a-bead models. Blue area represents the area between the upper and lower error bands for the interpolation curve. Data is presented as mean ± s.d. (n = 5), *p<0.05, **p<0.01, ***p<0.001.